Strong coupling superconductivity mediated by three-dimensional anharmonic phonons

K. Hattori[*] and H. Tsunetsugu

Institute for Solid State Physics, University of Tokyo, Kashiwanoha 5-1-5, Kashiwa, Chiba 277-8581, Japan

We investigate three-dimensional anharmonic phonons in tetrahedral symmetry and superconductivity mediated by these phonons. Three-dimensional anharmonic phonon spectra are calculated directly by solving Schrödinger equation and the superconducting transition temperature is determined by using the theory of strong coupling superconductivity assuming an isotropic gap function. With increasing the third-order anharmonicity b of the tetrahedral ion potential, we find a crossover in the energy spectrum to a quantum tunneling regime. We obtain strongly enhanced transition temperatures around the crossover point. We also investigate the anharmonic effects on the Debye-Waller factor, the phonon spectral functions and the density profile, as a function of the anharmonicity b and temperature. The isomorphic first-order transition observed in KOs_2O_6 is discussed in terms of the first excited state energy Δ and the coupling constant λ in the strong coupling theory of superconductivity. Our results suggest the decrease in λ and increase in Δ below the first-order transition temperature. We point out that the change in the oscillation amplitude $\langle x^2 \rangle$ and $\langle xyz \rangle$ characterizes this isomorphic transition. The chemical trends of the superconducting transition temperature, λ, and Δ in the β-pyrochlore compounds are also discussed.

I. INTRODUCTION

Recently, various low-energy properties arising from anharmonic ion oscillations have attracted much attention. An ion located at the center of an oversized cage oscillates with large amplitude and thus the anharmonic terms in the potential energy play an important role. Indeed, these anharmonic oscillations are observed in β-pyrochlore,[1–4] filled-skutterudite,[5–7] and clathrate compounds.[8–10] In metallic systems, such anharmonic oscillations interact with conduction electrons, and due to their large amplitude, the electron-phonon coupling constant becomes large. The large anharmonicity and the strong electron-phonon coupling lead unusual relaxation of conduction electrons,[3,11] anomalous nuclear magnetic relaxation time,[12,13] the sound velocity anomalies,[5,14–16] and the strong coupling superconductivity.[3,17–22]

These anharmonic oscillations in these systems have also been studied theoretically. Dahm and Ueda discussed the anomalous temperature dependence of the resistivity[1–3] and the NMR relaxation time[12] observed in KOs_2O_6 by using a single-site anharmonic phonon model, employing the self-consistent Gaussian approximation for the quartic term of the ion displacement.[23] Recently, Yamakage and Kuramoto extended this approach to the lattice problem in the same level of Gaussian approximation.[24] These works can explain the softening of optical-phonon frequency as temperature decreases observed in many compounds.[4,10,25–27]

The anharmonic ion oscillations had been discussed also as a possible mechanism of high transition temperature superconductivity, particularly for high-T_c cuprates.[28–31] As for the systems of anharmonic ion oscillations in oversized cages, importance of contributions of low-energy Pr ion oscillations to the superconductivity is pointed out in $PrOs_4Sb_{12}$.[21] Recently, Chang, *et al.*,[22] discussed the superconductivity in KOs_2O_6 using strong coupling theory of s-wave superconductivity[32] also employing the Gaussian approximation[23] for anharmonicity.

In this paper, we focus on the β-pyrochlore compounds AOs_2O_6 (A = K, Rb, or Cs). Monovalent A cations are located at the center of the $Os_{12}O_{18}$ cages and form a diamond lattice structure. Lattice dynamics was investigated by neutron-scattering experiments,[25–27] and a low-energy optical phonon is observed at about 3 meV in the K compound. This is basically K-cation oscillations and the same phonon is also observed at around 5–7 meV in the Rb and Cs compounds. The root-mean-square amplitude of the K oscillation turns out to be 0.12–0.14 Å at zero temperature from the elastic neutron scattering[25,26] while much smaller values are reported for Rb and Cs compounds.[25]

The first-principle calculations indicate that the K ion potential has large anharmonicity and is very shallow along [111] and three other equivalent directions.[33] It is also calculated that the first excited state has the excitation energy of ∼8 K and K-cation oscillation amplitude is as large as 1 Å at zero temperature. These values are quite different from the experimental data, indicating that some parameters in the ion potential are not so realistic. In the present paper, we will first systematically analyze the effects of anharmonicity of the ion potential on the ion dynamics in KOs_2O_6.

The β-pyrochlore compounds reveal superconducting phase transition and the transition temperature T_c's are 9.6 K, 6.3 K, and 3.3 K for A = K, Rb, and Cs, respectively. These values of T_c are inversely related to the A-cation size, i.e., T_c is the highest for the smallest ion: potassium. The symmetry of the gap function is considered to be fully gapped s wave.[12,18,19] It has been also shown that the electron-phonon coupling is large.[3,18,20] Thus, it is expected that the conduction electrons on the cages strongly interact with the anharmonic oscillations of ion inside the cage in these systems.

For KOs_2O_6, in addition to superconducting transition, there exists a first-order structural transition at T_p=7.5 K. At this transition, no sign of symmetry breaking has been observed.[3,4] The oscillation of K cation seems less anharmonic below T_p as indicated by electrical resistivity, specific-heat jump at T_c in magnetic fields and the mean-free

path estimated from the upper critical field H_{c2}.[3] Recently, we have proposed that this is driven by a sudden change in K-cation oscillation amplitude driven by intersite ion interactions.[34] The amplitude of the low-energy excited state with xyz symmetry jumps at T_p but this does not change the T_d point-group symmetry.

The main purpose of this paper is to clarify the properties of anharmonic oscillations in tetrahedral symmetry, which is the local symmetry for A cations in AOs_2O_6, and the superconductivity mediated by these anharmonic oscillations. In order to fully take into account the anharmonicity and anisotropy, we will solve the three-dimensional Schrödinger equation for an anharmonic oscillator in the tetrahedral symmetry. Using these exact phonon eigenstates, we will then discuss the strong coupling superconductivity assuming an s-wave pairing.

This paper is organized as follows. In Sec. II, we will calculate the energy spectrum of the anharmonic potential problem and discuss various thermodynamic and dynamical quantities and their dependence on temperature. Anharmonic effects on Debye-Waller factor will also be discussed. Section III is devoted to the discussions for strong coupling superconductivity mediated by the anharmonic ion oscillations discussed in Sec. II. In Sec. IV, we will discuss the relevance of the present results to the β-pyrochlore compounds. We also apply our theory to discuss the changes in phonon dynamics at the first-order transition at T_p. Finally Sec. V is a summary of this paper.

II. ANHARMONIC PHONONS

A. Model

In this paper, we investigate an anharmonic oscillation of K ion in KOs_2O_6. Our model is anharmonic local phonons at each lattice point and we assume the local symmetry is tetrahedral one which corresponds to the case of K-site symmetry in KOs_2O_6. In tetrahedral symmetry, in addition to spherical and cubic fourth-order terms, there exists a third-order anharmonic term which breaks inversion symmetry and the Hamiltonian is given by

$$H = -\frac{\hbar^2}{2M}\nabla_{\mathbf{R}}^2 + V(\mathbf{R}), \tag{1}$$

$$V(\mathbf{R}) = \frac{1}{2}M\Omega_0^2|\mathbf{R}|^2 + BXYZ + C_1|\mathbf{R}|^4 + C_2(X^4 + Y^4 + Z^4), \tag{2}$$

where $\mathbf{R} = (X, Y, Z)$ is the real-space displacement of the ion from the equilibrium position. M is the mass of the ion. Throughout this paper we set $M/m_e = 71748$, where m_e is the mass of electron, except for discussions in Sec. IV A, and this corresponds to the mass of K ion. Ω_0 and B are coefficients of second- and third-order terms in the ion potential, while C_1 and C_2 are isotropic and cubic fourth-order terms, and we ignore the higher-order potential terms of $O(R^5)$. To study dependence on potential parameters, it is useful to rewrite Hamiltonian (1) into a dimensionless form by renor-

malizing displacement and energy by their units. As for the energy unit, we choose the energy of harmonic phonon corresponding the second-order term $\hbar\Omega_0$. The unit of the length is chosen as $a_0 \equiv \hbar/M\Omega_0 = a_B\sqrt{2(e^2/2a_B)(m_e/M)/\hbar\Omega_0}$. Here, a_B is the Bohr radius $a_B = \hbar^2/m_e e^2 \simeq 0.53$ Å.

In these units, Hamiltonian (1) is transformed to

$$\bar{H} \equiv \frac{H}{\hbar\Omega_0} = -\frac{1}{2}\nabla_{\mathbf{r}}^2 + \bar{V}(\mathbf{r}), \tag{3}$$

$$\bar{V}(\mathbf{r}) = \frac{1}{2}\omega_0|\mathbf{r}|^2 + bxyz + c_1|\mathbf{r}|^4 + c_2(x^4 + y^4 + z^4), \tag{4}$$

where $\mathbf{r} = (x, y, z) = \mathbf{R}/a_0$. b and c_1 and c_2 are dimensionless constants and ω_0 is introduced to vary the second-order term for later purpose but $\omega_0 = 1$ for the main part of this paper. In Secs. III and IV, we will use different values of ω_0 to examine the effects of changes in the second-order term.[35] Throughout this paper we set $\hbar\Omega_0 = 44$ K which corresponds to the energy scale of the optical-phonon frequency observed in β-pyrochlore compounds,[3,25,27] and thus $a_0 \simeq a_B/\sqrt{10}$.

In the limit of $b = c_1 = c_2 = 0$, Hamiltonian (3) can be diagonalized by using creation and annihilation operators as,

$$\bar{H} = a_x^\dagger a_x + a_y^\dagger a_y + a_z^\dagger a_z + \frac{3}{2}, \tag{5}$$

where $a_\mu \equiv \frac{1}{\sqrt{2}}(\partial_\mu + x_\mu)$ with $\mu = x$, y, or z. Eigenstates are labeled by three occupation numbers as $\bar{H}|n_x, n_y, n_z\rangle = (n_x + n_y + n_z + 3/2)|n_x, n_y, n_z\rangle$ and $a_\mu^\dagger a_\mu|n_x, n_y, n_z\rangle = n_\mu|n_x, n_y, n_z\rangle$.

For nonzero b, c_1, and c_2, we diagonalize Hamiltonian (3) numerically in the restricted Hilbert space spanned by $\{|n_x, n_y, n_z\rangle\}$ with $n_x + n_y + n_z \leq n_{max}$. In this paper, we use $n_{max} = 40$ which corresponds to the Hilbert space with 12341 states and check the convergence by comparing the results for $n_{max} = 50$ including 23426 states. We employ this approach rather than the conventional self-consistent Gaussian approximation.[23,24] This is because the conventional approximation does not work for the potential, Eq. (4), since the third-order term cannot be decoupled as in the fourth-order terms. It is also important that, as will be shown later, energy differences between adjacent eigenstate multiplets are not the same, and this property cannot be described by the self-consistent Gaussian approximation.

B. Energy spectrum

In Fig. 1, we show a low-energy part of the energy spectra of Hamiltonian (3) as a function of the third-order anharmonicity b for $c_1 = 0.04$ and $c_2 = 0.01$. The ground state is always nodeless in the space $\mathbf{r}$ and therefore singlet, while the first excited states are triplet, corresponding to s and p orbitals for the case of isotropic potential. As b increases, the energy of the lowest singlet excited state (hereafter, this state will be referred to as s' state) decreases and shows an anticrossing with the ground state at $b = b^* \sim 1.7$. This kind of anticrossing behavior does not occur in the one-dimensional anharmonic potential problem: $V(X) = aX^2 + bX^4$.[10,23] Interestingly, near $b = b^*$ the five lowest-energy states are well separated from other states in the energy spectra. Thus, the validity of our
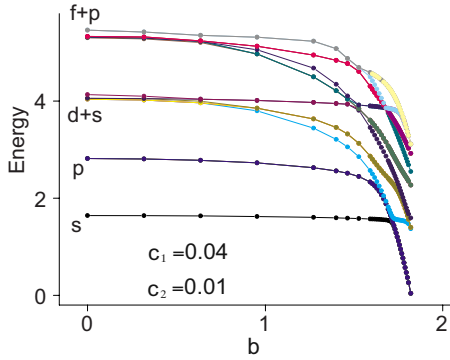
FIG. 1. (Color online) Energy eigenvalues vs the third-order anharmonic parameter b for $c_1 = 0.04$ and $c_2 = 0.01$. s, p, d, and f denote the approximate orbital symmetry, which is exact in the isotropic harmonic potential case.

previous five-state toy model is justified around this cross-over region.[34]

For $b > b^*$, the excited triplet states, which are p-wavelike, are nearly degenerate with the ground state. This means that these four states are localized away from the origin in the four directions: $[\bar{1}\bar{1}\bar{1}]$, $[11\bar{1}]$, $[\bar{1}11]$, and $[1\bar{1}1]$. For the illustration, we show the potential form along [100], [110], and [111] directions in Fig. 2. It is clear that an off-center potential local minimum emerges along [111] direction as b increases. The energy of the first excited state from the ground state Δ is small, owing to smallness of the quantum tunneling probability between different valleys. These four states form sp^3 orbitals and their energy can be well described by considering the quantum tunneling of the ion between the four potential minimum positions. Hereafter, we call these states in this parameter region ($b > b^*$) as *quantum tunneling states*.

C. Observables

We now investigate the temperature dependence of the oscillation amplitude of these anharmonic ions. Thermodynamic average of observable A is calculated by the formula,

$$\langle A \rangle = \sum_n w_n \langle n|A|n\rangle, \qquad (6)$$

where $|n\rangle$ is the eigen state of Hamiltonian (1) with eigen-energy E_n and w_n is its Boltzmann weight w_n
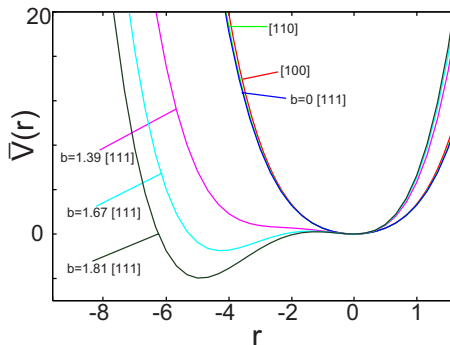

FIG. 2. (Color online) Potential along [100], [110], and [111] directions for various b. $c_1 = 0.04$ and $c_2 = 0.01$. $\mathbf{r} = r\mathbf{n}$, where $\mathbf{n}$ being the unit vector along each direction.
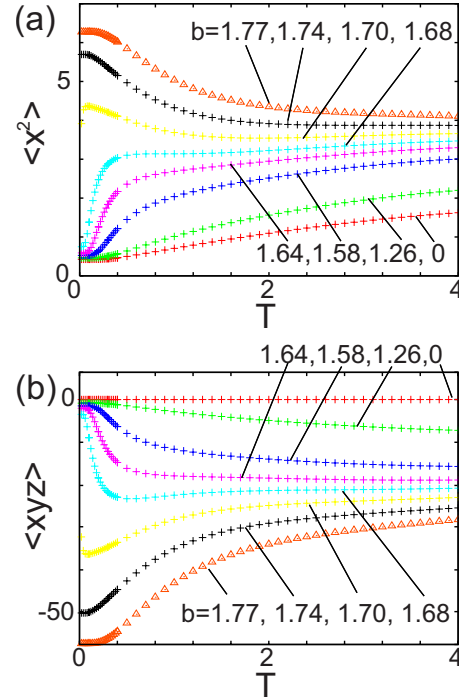

FIG. 3. (Color online) Temperature dependence of thermodynamic average (a) $\langle x^2 \rangle$ and (b) $\langle xyz \rangle$. $c_1 = 0.04$ and $c_2 = 0.01$.

$= \exp(-E_n/T)/\Sigma_m \exp(-E_m/T)$, and T is the temperature. In the summation in Eq. (6), we discard states with $E_n > 0.8 n_{\max}\omega_0$, since the high-energy parts of our energy spectrum is not correct due to the cutoff $n_{\max}$ and the high-energy part does not matter as long as the low-temperature properties of the system are concerned.

In Fig. 3, we show the temperature dependence of fluctuations $\langle x^2 \rangle = \langle \mathbf{r}^2 \rangle / 3$ and $\langle xyz \rangle$. Note that since xyz is invariant quantity in tetrahedral symmetry, this does not vanish except for $b = 0$. As the temperature decreases, both $\langle x^2 \rangle$ and $|\langle xyz \rangle|$ decrease and saturate to finite values for $b < b^*$. On the other hand, for $b > b^*$, these quantities increase at low temperatures suggesting the quantum tunneling state.

To see the change with b more clearly, we calculate the ion density $\rho(\mathbf{r}) \equiv \Sigma_n w_n |\Psi_n(\mathbf{r})|^2$ at position $\mathbf{r}$. Here $\Psi_n(\mathbf{r})$ is the wave function at position $\mathbf{r}$ which is normalized as $\int d^3x |\Psi_n(\mathbf{r})|^2 = 1$. In Figs. 4(a)–4(d), we show $\rho(\mathbf{r})$ along [111] direction, $\mathbf{r} = r(1,1,1)/\sqrt{3}$, for several temperatures. $\rho(\mathbf{r})$ in other directions has monotonic temperature dependence and is peaked at $\mathbf{r} = (0,0,0)$ as in Fig. 4(a). As b increases, a part of the weight of $\rho(\mathbf{r})$ shifts to the position around $r \sim -4$. Interestingly near $b = b^*$ [Fig. 4(c)], the temperature dependence of $\rho(\mathbf{r})$ at $r \sim -4$, is nonmonotonic, i.e., as T decreases, $\rho(-4)$ increases first, but decreases below $T \sim 0.3 \sim \Delta$. In Fig. 4(d), the $\rho(0)$ is suppressed at low temperatures reflecting the nature of the quantum tunneling states, since the potential minimum away from the origin is deep enough as shown in Fig. 2.

D. Debye-Waller factor

Now we discuss the Debye-Waller factor, which contains information about the amplitude of ion oscillation and it is
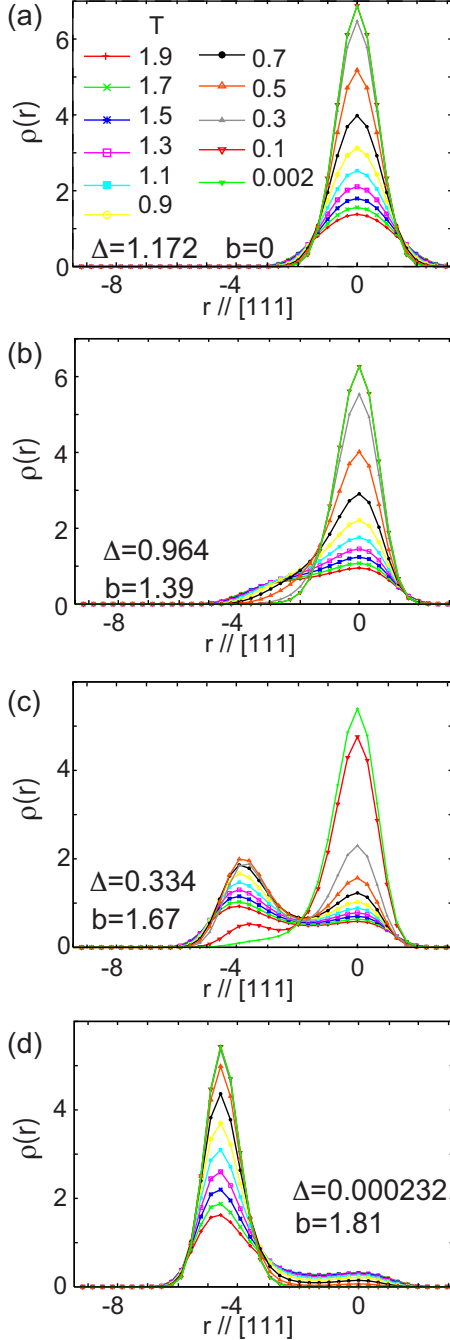
FIG. 4. (Color online) Atomic density profile $\rho(\mathbf{r})$ along $\mathbf{r} = r(1,1,1)/\sqrt{3}$ for various b. $c_1 = 0.04$ and $c_2 = 0.01$.

observed by elastic neutron-scattering experiments.[36] Consider an atom whose position is represented by $\mathbf{d}$ in a unit cell and denote its displacement by $\mathbf{u_d} = (u_\mathbf{d}^x, u_\mathbf{d}^y, u_\mathbf{d}^z)$. Then, the Debye-Waller factor at the scattering wave vector $\mathbf{Q}$ for this atom $e^{-W_\mathbf{d}(\mathbf{Q})}$ is given by

$$\exp[-W_\mathbf{d}(\mathbf{Q})] = \langle \exp(-i\mathbf{Q} \cdot \mathbf{u_d}) \rangle. \tag{7}$$

In the harmonic approximation, Eq. (7) reduces to

$$W_\mathbf{d}^{(2)}(\mathbf{Q}) = \frac{1}{2}\langle (\mathbf{Q} \cdot \mathbf{u_d})^2 \rangle. \tag{8}$$

Using $W_\mathbf{d}(\mathbf{Q})$, the static structure factor $F(\mathbf{Q})$ is represented as

$$F(\mathbf{Q}) = \sum_\mathbf{d} \bar{b}_\mathbf{d} \exp(i\mathbf{Q} \cdot \mathbf{d})\exp[-W_\mathbf{d}(\mathbf{Q})], \tag{9}$$

where $\bar{b}_\mathbf{d}$ is the averaged scattering length of the atom at position $\mathbf{d}$.

When anharmonicity is not negligible, Eq. (8) is not sufficient and we must take into account higher-order terms. Up to the third order in $(\mathbf{Q} \cdot \mathbf{u_d})$, we obtain

$$W_\mathbf{d}^{(3)}(\mathbf{Q}) = \frac{1}{2}\langle (\mathbf{Q} \cdot \mathbf{u_d})^2 \rangle + \frac{i}{6}\langle (\mathbf{Q} \cdot \mathbf{u_d})^3 \rangle. \tag{10}$$

As an example, let us consider K atoms in KOs_2O_6, which constitute a diamond sublattice. There are two sites in the unit cell, $\mathbf{d}_A = (0,0,0)$ and $\mathbf{d}_B = \frac{a}{4}(1,1,1)$. Here a is the lattice constant. From the symmetry arguments, we obtain

$$\frac{1}{2}\langle (\mathbf{Q} \cdot \mathbf{u_d})^2 \rangle = \frac{1}{6}|\mathbf{Q}|^2\langle |\mathbf{u_d}|^2 \rangle \equiv W_\mathbf{d}', \tag{11}$$

$$\frac{1}{6}\langle (\mathbf{Q} \cdot \mathbf{u_d})^3 \rangle = Q_x Q_y Q_z \langle u_\mathbf{d}^x u_\mathbf{d}^y u_\mathbf{d}^z \rangle \equiv W_\mathbf{d}''. \tag{12}$$

In the diamond lattice structure, $W_{\mathbf{d}_A}'(\mathbf{Q}) = W_{\mathbf{d}_B}'(\mathbf{Q}) \equiv W'(\mathbf{Q})$ and $W_{\mathbf{d}_A}''(\mathbf{Q}) = -W_{\mathbf{d}_B}''(\mathbf{Q}) \equiv W''(\mathbf{Q})$. Using Eqs. (11) and (12) and setting $\bar{b} \equiv \bar{b}_{\mathbf{d}_A} = \bar{b}_{\mathbf{d}_B}$, we obtain

$$|F(\mathbf{Q})|^2 = 2\bar{b}^2 \exp[-2W'(\mathbf{Q})]$$
$$\times \{1 + \cos[\mathbf{Q} \cdot (\mathbf{d}_A - \mathbf{d}_B) - 2W''(\mathbf{Q})]\}. \tag{13}$$

Thus, the effective $W(\mathbf{Q})$ becomes

$$W_{\text{eff}}(\mathbf{Q}) = W'(\mathbf{Q}) - \frac{1}{2}\log 2$$
$$- \log\left|\cos\left[\frac{1}{2}\mathbf{Q} \cdot (\mathbf{d}_A - \mathbf{d}_B) - W''(\mathbf{Q})\right]\right|. \tag{14}$$

It is important to note that since the $W''(\mathbf{Q})$ depends on the wave vector as $Q_x Q_y Q_z$, the effect of anharmonicity is anisotropic. For example, at $\mathbf{Q}_{111} = (1,1,1)2\pi/a$, W_{eff} is given by

$$W_{\text{eff}}(\mathbf{Q}_{111}) = W_{\text{eff}}(-\mathbf{Q}_{111})$$
$$= W'(\mathbf{Q}_{111}) - \frac{1}{2}\log\{1 + \sin[2W''(\mathbf{Q}_{111})]\}, \tag{15}$$

whereas at $\mathbf{Q}_{200} = (2,0,0)2\pi/a$, we obtain

$$W_{\text{eff}}(\mathbf{Q}_{200}) = W'(\mathbf{Q}_{200}) = \frac{4}{3}W'(\mathbf{Q}_{111}). \tag{16}$$

The third-order contribution $\langle u_\mathbf{d}^x u_\mathbf{d}^y u_\mathbf{d}^z \rangle$ also modifies the extinction rule of the structure factor. According to Eq. (13), $|F(\mathbf{Q})|^2 = 0$ at $\mathbf{Q} = (2,0,0)2\pi/a$ and also at $(2,2,2)2\pi/a$ due to the interference factor $1 + \cos[\mathbf{Q} \cdot (\mathbf{d}_A - \mathbf{d}_B)]$ when $W''(\mathbf{Q})$
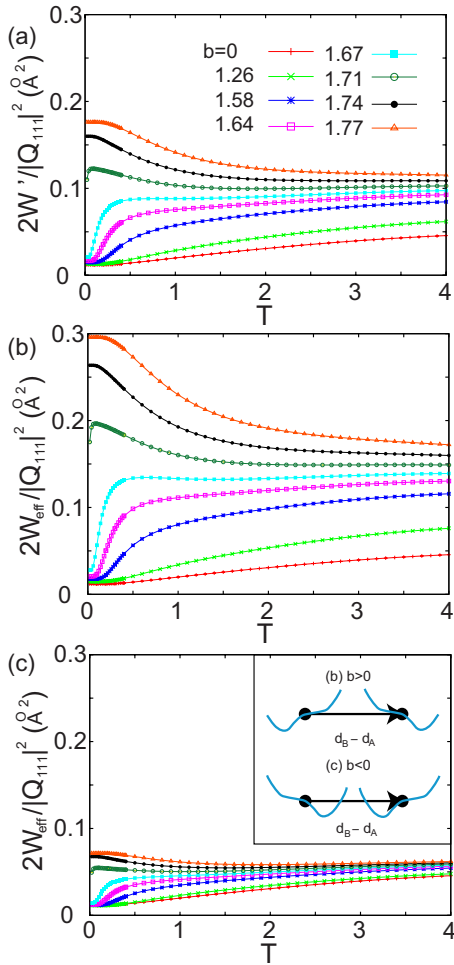
FIG. 5. (Color online) Temperature dependence of the exponent of the Debye-Waller factor for $c_1=0.04$ and $c_2=0.01$. (a) $W'(\mathbf{Q}_{111})$. (b) $W_{\text{eff}}(\mathbf{Q}_{111})$ for $b>0$. (c) $W_{\text{eff}}(\mathbf{Q}_{111})$ for $b<0$. Inset in (c): schematic potential form along the [111] direction in (b) and (c) for large b cases.
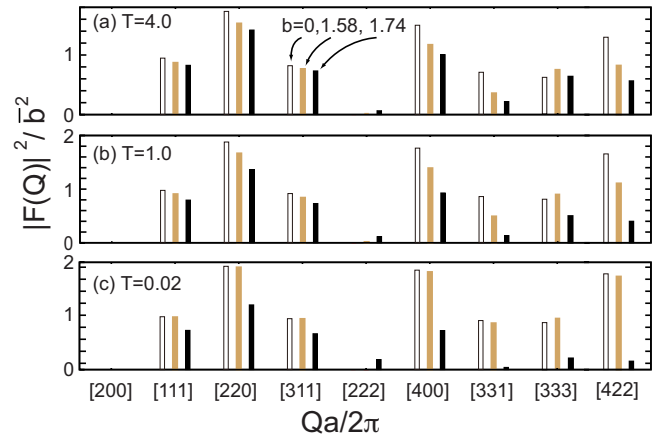

FIG. 6. (Color online) $\mathbf{Q}$ dependence of $|F(\mathbf{Q})|^2$ for $c_1=0.04$ and $c_2=0.01$ at temperatures (a) $T=4.0$, (b) $T=1.0$, and (c) $T=0.02$. For each of $\mathbf{Q}$, $|F(\mathbf{Q})|^2$ values for $b=0$, 1.58, and 1.74 are shown from left to right. For $\mathbf{Q}=2\pi(2,0,0)/a$, $|F(\mathbf{Q})|^2$ is always zero.

is set to be zero. For $b\neq 0$, $\langle u_\mathbf{d}^x u_\mathbf{d}^y u_\mathbf{d}^z \rangle$ is finite and this leads to nonvanishing $W''(\mathbf{Q})$ at $\mathbf{Q}=(2,2,2)2\pi/a$ but $W''(\mathbf{Q})=0$ at $\mathbf{Q}=(200)2\pi/a$, since $W''(\mathbf{Q})$ is proportional to $Q_x Q_y Q_z$. Therefore, $|F(\mathbf{Q})|^2$ is nonvanishing at $\mathbf{Q}=(2,2,2)2\pi/a$ while remains zero at $\mathbf{Q}=(2,0,0)2\pi/a$.

We show the calculated $W_{\text{eff}}(\mathbf{Q}_{111})$ for several values of b as a function of temperature in Fig. 5. In Fig. 5(a), the first term in Eq. (15) is shown and $W_{\text{eff}}(\mathbf{Q}_{111})$ for $b>0$ and $b<0$ are shown in (b) and (c), respectively. It is easily seen that, for small b, $W_{\text{eff}}(\mathbf{Q}_{111})$ in Figs. 5(b) and 5(c) are essentially the same as $W'(\mathbf{Q}_{111})$ in (a), while, for larger b, $W_{\text{eff}}(\mathbf{Q}_{111})$ is enhanced (suppressed) for $b>0$ in (b) [$b<0$ in (c)]. For other directions of $\mathbf{Q}$ with $Q_x Q_y Q_z=0$, $W_{\text{eff}}(\mathbf{Q})$ does not include the contribution of the third-order term $W''(\mathbf{Q})$ and thus, $W_{\text{eff}}=W'$.

Figure 6 shows the wave-vector dependence of $|F(\mathbf{Q})|^2$ for several temperatures and b. Note that $F(\mathbf{Q})$ at $\mathbf{Q}=(2,0,0)2\pi/a$ vanishes due to the extinction rule mentioned above while the intensity at $\mathbf{Q}=(2,2,2)2\pi/a$ appears for nonzero b although its strength is weak. Concerning b dependence, $|F(\mathbf{Q})|^2$ for $b=1.74$ is much suppressed for large

$|\mathbf{Q}|$ and low temperatures, which is originated from the large displacement for $b>b^*$. As for the temperature dependence, $|F(\mathbf{Q})|^2$ increases as T decreases for $b=0$ and 1.58, while decreases for $b=1.74>b^*$. This temperature dependence of $|F(\mathbf{Q})|^2$ for $b>b^*$ is also understood from the temperature dependence of W_{eff} in Fig. 5, where W_{eff} for larger $b>b^*$ increases as T decreases.

We note that by careful analysis of the neutron data, as we have demonstrated the effects of the third-order term on the Debye-Waller factor, we can obtain useful information about anharmonicity in the real materials. In KOs_2O_6, since there are a lot of kinds of atoms such as the oxygen and osmium, our results presented in this section cannot directly be compared with the neutron data of KOs_2O_6. It is desired to carry out high-resolution neutron-scattering experiments using the single crystal and analyze the results by taking into account the anharmonicity.

E. Ion dynamics

Now let us investigate the dynamics of the anharmonic ion oscillation. In Fig. 7, we show the phonon density of states (DOS) $F(\omega)$, which is calculated from the correlation function D,

$$D_{\mu\mu'}(\omega) = \sum_{nm} (w_n - w_m) \frac{\langle n|x_\mu|m\rangle\langle m|x_{\mu'}|n\rangle}{\omega - E_m + E_n + i\eta}. \quad (17)$$

The DOS is given by its imaginary part, $F(\omega) = -\text{Im}\, D_{xx}(\omega)/\pi$. Notice $D_{xx}(\omega) = D_{yy}(\omega) = D_{zz}(\omega)$ in the tetrahedral symmetry. We set the phenomenological broadening parameter $\eta=0.26$. Although one can try more sophisticated analyses by introducing dissipation by electron-phonon couplings or couplings with other degrees of freedom to calculate the imaginary part of the self-energy $\eta(\omega)$,[37,38] it is sufficient at this stage to restrict ourselves in the phenomenological level as long as characteristic properties of the DOS are concerned.

Figure 7(a) shows the phonon DOS $F(\omega)$ for the case $b=0$ and the eigenenergies relative to the ground-state energy
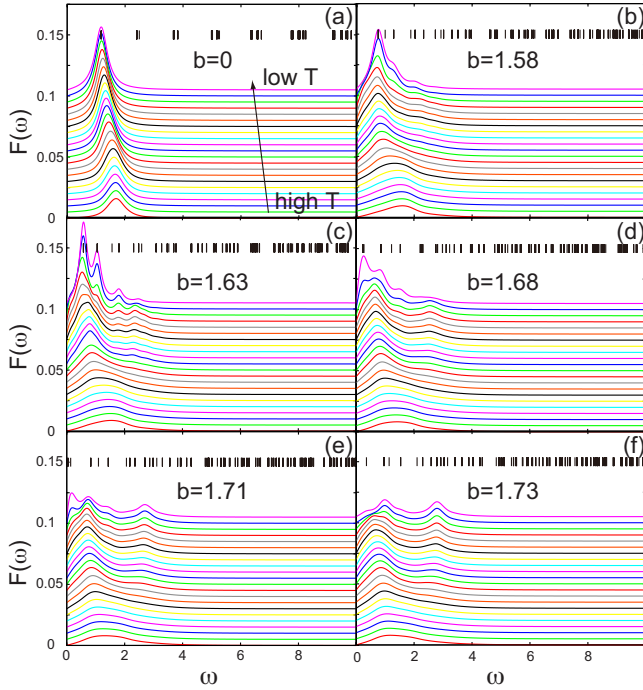
FIG. 7. (Color online) Phonon DOS $F(\omega)$ for various b's fixing $c_1 = 0.04$ and $c_2 = 0.01$. The data correspond to $T = 10$, 9.2, 8.4, 7.6, 6.8, 6.0, 5.2, 4.4, 3.6, 2.8, 2.0, 1.8, 1.6, 1.4, 1.2, 1.0, 0.8, 0.6, 0.4, 0.2, and 0.1, from bottom to top and each curve is shifted up by 0.005. Energy eigenvalues relative to the energy of the ground state are shown by short bars in each panel.

indicated by small bars. It is clearly seen that the position of the peak decreases as the temperature decreases and this softening is consistent with the study based on self-consistent Gaussian approximations.[23,24] The single peak in $F(\omega)$ is actually constituted of many Lorentzian peaks each of which has a width of $\eta = 0.26$. In this case of $b = 0$, the transition matrix elements are sizable only between neighboring "multiplets" of the corresponding harmonic system. Because of the fourth-order anharmonicity, c_1 and c_2, the degeneracy of each multiplet is only approximate and slightly lifted, and also the energy separation between multiplets increases with increasing energy. Since the distribution of Lorentzian peak positions is quite smooth and the energy dependence of Boltzmann weight is monotonic, they finally form a single broad peak. Its position shifts from a low energy at low T where only the ground state is an important initial state to a higher energy at higher T where higher excited states contribute more importantly.

For $b > 0$, qualitatively different behaviors appear as shown in Figs. 7(b)–7(f). The transition matrix elements are now finite for many more pairs of eigenstates $\langle n|x|m \rangle$ for nonzero b. This is because the point-group symmetry changes from cubic O_h to tetrahedral T_d and the eigenstates $|n\rangle$ do not have definite parity related to inversion symmetry $\mathbf{r} \to -\mathbf{r}$. In this point-group symmetry, for example, x and yz are bases of the same T_2 irreducible representation. As a result, the matrix element such as $\langle yz|x|s \rangle$ is nonvanishing (here "s" means an isotropic s-wave state, i.e., A_1 in T_d point group). In particular, the ground state has transition matrix

elements much larger than in the case of $b = 0$. Thus, even at the lowest temperature, more than one peaks are present in $F(\omega)$ for $b > 0$, while the $b = 0$ case has no additional visible high-energy peak in $F(\omega)$ as shown in Fig. 7(a), since the ground state has nonvanishing matrix elements only with the odd-parity excited states and their magnitude is small.

For clarity, let us concentrate on a few specific peaks to understand their origin for $b \neq 0$. $F(\omega)$ for the lowest temperature $T = 0.1$ in Fig. 7(c) shows four peaks below $\omega \sim 3$. As it is easily checked by comparing the energy eigenvalues indicated by bars in Fig. 7, the positions of these peaks correspond to the excitation energies. Actually, the lowest three peaks in Fig. 7(c) correspond to the transitions to the T_2 states which can be traced back to the p-wave sates in the one-phonon multiplet, the d-wave states in the two-phonon multiplet, and the p- or f-wave states in the three-phonon multiplet in the harmonic oscillator (see Fig. 1 where the label of the multiplets in the harmonic oscillator are indicated).

There are also peaks or shoulderlike structures originating from the transition between the s' and T_2 states for $b > 0$. Among them, the transition between the first excited p-wave states to s' state is clearly seen in Figs. 7(b) and 7(c). Since the energy difference between these excited states Δ' is smaller than that between the ground state and the first excited state Δ, these shoulderlike structures appear at energies lower than the main peak position which corresponds to the transition from the ground state and the first excited states for the intermediate temperatures. In Fig. 7(d), Δ' is so small that the structure at $\omega \sim \Delta'$ is not clearly visible but the slope $F(\omega)/\omega$ near $\omega \sim 0$ is enhanced. In Figs. 7(e) and 7(f), the first excited states are almost degenerate with the ground state, so that the lowest-energy peak in the figures does not correspond to the transition to the first excited states but that between the first excited states and s' state.

III. STRONG COUPLING SUPERCONDUCTIVITY

In this section, we will discuss the strong coupling theory of superconductivity[39,40] in which the attractive force between electrons is mediated by the anharmonic phonons discussed in the previous section. The main issue of this section is the effect of the phonon anharmonicity on the superconducting transition temperature T_c.

We assume that the phonon DOS is given by $F(\omega)$ obtained in Sec. II E, i.e., we ignore the renormalization due to the electron-phonon coupling. Generally, electron-phonon couplings lead to frequency renormalization and a finite lifetime of phonons, both of which are described in the renormalization of $F(\omega)$. This renormalization is interesting and generally should be included but the present calculation reproduces correct qualitative behaviors and we leave full self-consistent calculation as a future problem. It is noted that the frequency renormalization is taken into account such that the potential parameters are chosen to reproduce a renormalized frequency. The superconducting transition temperature T_c is obtained by applying the conventional strong coupling theory of s-wave pairing[39,40] to our anharmonic phonon system coupled to isotropic electron gas.

Throughout this section, we use Matsubara formalism, which is efficient to determine T_c. Matsubara formulation has also advantage that the phenomenological broadening factor η used in Sec. II E is not necessary.

A. Gap equations

Following the conventional theory of strong coupling superconductivity,[41] the transition temperature T_c for isotropic s-wave gap Δ_{SC} is determined by the gap equation,

$$\Delta_{SC}(i\epsilon_m) = -\alpha^2 T \sum_n K(i\epsilon_n) D(i\epsilon_m - i\epsilon_n)\Delta_{SC}(i\epsilon_n), \quad (18)$$

$$K(i\epsilon_n) = \int_{-\infty}^{\infty} d\xi\, G(\xi, i\epsilon_n) G(\xi, -i\epsilon_n), \quad (19)$$

where the electron Green's function is given by

$$G(\xi, i\epsilon_n) = \frac{1}{i\epsilon_n - \xi - \Sigma(i\epsilon_n)}, \quad (20)$$

and the normal self-energy is given by

$$\Sigma(i\epsilon_n) = -\alpha^2 T \sum_m \int_{-\infty}^{\infty} d\xi\, G(\xi, i\epsilon_n - i\nu_m) D(i\nu_m). \quad (21)$$

Here $D(i\nu_m) = D_{\mu\mu}(i\nu_m)$ is the phonon Green's function. $\epsilon_n = (2n+1)\pi T$ and $\nu_m = 2m\pi T$ are the fermionic and bosonic Matsubara frequencies, respectively. α^2 is proportional to the square of the electron-phonon coupling constant times electron DOS at Fermi energy. In our model, it is a frequency-independent quantity and is set as $\alpha^2 = 595$ K/Å^2, which corresponds to 0.38 in our units of energy and length. As in the conventional theory,[39,40] the normal self-energy, Eq. (21), is essentially given by the second-order perturbation theory and $K(i\epsilon_n)$ is analytically given by[42]

$$K(i\epsilon_n) = \left| \frac{\epsilon_n}{\pi} - \alpha^2 T \left[2\sum_{m=1}^{n} D(i\nu_m) + D(0) \right] \right|^{-1}. \quad (22)$$

To determine T_c, we define

$$\mathcal{M}_{mn} \equiv -\alpha^2 T \sqrt{K(i\epsilon_m)} D(i\epsilon_m - i\epsilon_n) \sqrt{K(i\epsilon_n)} \quad (23)$$

$$= \mathcal{M}_{nm}, \quad (24)$$

$$\psi_n \equiv \Delta_{SC}(i\epsilon_n)\sqrt{K(i\epsilon_n)}, \quad (25)$$

and solve eigenvalue problem numerically

$$\Lambda(T)\psi_m = \sum_n \mathcal{M}_{mn}\psi_n. \quad (26)$$

With decreasing temperature, $\Lambda(T)$ increases and T_c is given by the condition: $\Lambda(T_c) = 1$.

B. Superconducting transition temperature in harmonic systems

Before discussing the effects of phonon anharmonicity on T_c, we show in Fig. 8 T_c in the harmonic system as a function
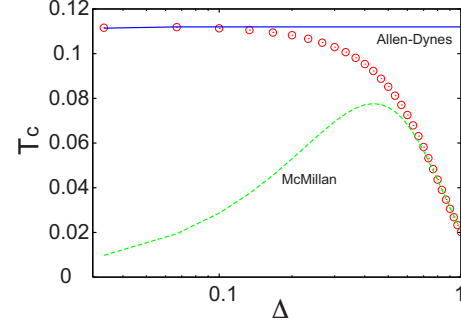

FIG. 8. (Color online) Superconducting transition temperature T_c vs the phonon energy Δ for the harmonic case $b = c_1 = c_2 = 0$. The dashed line corresponds to T_c^M given by Eq. (27) and the solid line represents T_c^{AD} given by Eq. (31).

of the first excited state energy $\Delta = \omega_0$. The dash line is T_c calculated by McMillan's formula,[43] which is valid in the weak-coupling regime, while the solid line is that by Allen and Dynes,[44] which gives a good estimation of T_c in the extremely strong coupling regime. Let us summarize two analytic formulae for the two opposite limits. The McMillan's formula is given by

$$T_c^M = 0.8\omega_{\log} \exp\left(-\frac{1+\lambda}{\lambda}\right), \quad (27)$$

where the Coulomb pseudopotential is not taken into account. Here, the dimensionless coupling constant λ is given by

$$\lambda \equiv \alpha^2 \int_{-\infty}^{\infty} d\omega\frac{F(\omega)}{\omega} = \alpha^2 \sum_{n,m} \frac{w_n - w_m}{E_m - E_n}|\langle n|x|m\rangle|^2, \quad (28)$$

and the characteristic energy scale $\omega_{\log}$ is given by

$$\log \omega_{\log} = \frac{2\alpha^2}{\lambda} \int_0^{\infty} d\omega\frac{F(\omega)}{\omega}\log\omega \quad (29)$$

$$= \frac{2\alpha^2}{\lambda} \sum_{E_m > E_n} \frac{w_n - w_m}{E_m - E_n}|\langle n|x|m\rangle|^2 \log(E_m - E_n). \quad (30)$$

The Allen-Dynes formula is given by

$$T_c^{AD} = 0.18\sqrt{\lambda\langle\omega^2\rangle}, \quad (31)$$

where $\langle\omega^2\rangle = 2\alpha^2 \int_0^{\infty} \omega F(\omega)d\omega/\lambda$.

In the case of harmonic phonons, λ can be analytically calculated and is given by $\lambda = \alpha^2/\Delta^2$.[45] This means the smaller Δ is, the larger λ is realized. The McMillan's formula (27) indeed reproduces T_c for large Δ as expected, while for small Δ, T_c approaches the value of the Allen-Dynes formula (31) ($= 0.18\sqrt{0.38} \simeq 0.11$) as shown in Fig. 8. Note that for the harmonic phonons, $\langle\omega^2\rangle = \Delta^2$. This relation is valid only for harmonic oscillators as will be discussed below.
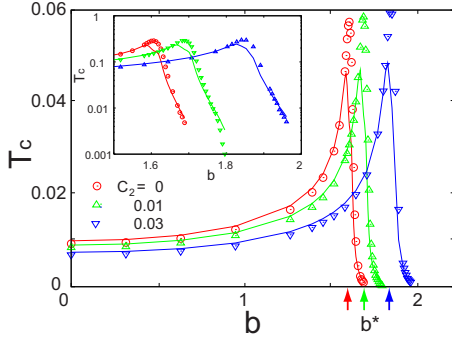
FIG. 9. (Color online) T_c vs b for $c_1 = 0.04$ and $c_2 = 0$, 0.01, and 0.03. The solid lines show T_c's of McMillan's formula (27). b^*'s for each of c_2 are indicated by arrows. Inset: zoom up in the large b part.

FIG. 10. (Color online) λ, $\omega_{\log}$, and Δ vs b for $c_2 = 0$, 0.01, and 0.03. The open symbols represent λ and the filled symbols with a solid line represent $\omega_{\log}$. Lines without symbols represent Δ. λ and $\omega_{\log}$ are calculated at $T = T_c$.

C. Superconducting transition temperature in anharmonic systems

Now, we discuss the effects of anharmonicity of phonon dynamics on T_c. Figure 9 shows the dependence of T_c on the third-order anharmonic term b of the ion potential, Eq. (4), for $c_2 = 0$, 0.01, and 0.03, at fixed $c_1 = 0.04$. All the three cases exhibit a pronounced peak around the crossover value $b = b^*$ as discussed in Sec. II for each c_2, and T_c's are strongly suppressed in the quantum tunneling states, i.e., for large $b > b^*$. The solid lines in the figure represent the McMillan's formula T_c^M [Eq. (27)]. The agreement with the McMillan's formula indicates that T_c is qualitatively given by the conventional theory of strong coupling superconductivity. Note that λ and $\omega_{\log}$ vary with the temperature in the presence of anharmonicity and T_c^M are calculated by using these values evaluated at $T = T_c$. For $b \gtrsim b^*$, however, the discrepancy becomes large as shown in the inset of Fig. 9, and the effects of anharmonicity and the nature of the extreme strong coupling regime appear, which will be discussed later in Sec. III E.

D. Competition between the energy scale and coupling constant

In Sec. III D, we discuss the origin of the peak structure based on the McMillan formula.[43] The McMillan's formula is expressed with the two parameters, λ and $\omega_{\log}$, as shown in Eq. (27). In Fig. 10, we show the b dependence of λ and $\omega_{\log}$ calculated at T_c together with Δ. It is noticeable that λ shows a steep increase above b^* and $\omega_{\log}$ is almost the same as Δ for $b \lesssim b^*$. From these facts, one can easily understand that T_c calculated by Eq. (27) decreases in the quantum tunneling states. The peak structure in T_c in Fig. 9 is a result of the competition between the suppression of $\omega_{\log}(\Delta)$ and the enhancement of λ. Thus, the peak structure is realized at $b \simeq b^*$, where λ is large enough and simultaneously $\omega_{\log}$ is not vanishingly small.

E. Strong coupling limit

In an extreme strong coupling regime $\lambda \gg 1$, Allen and Dynes showed that T_c is approximately given by Eq. (31) rather than the McMillan's formula (27).[44] When Eq. (31) is
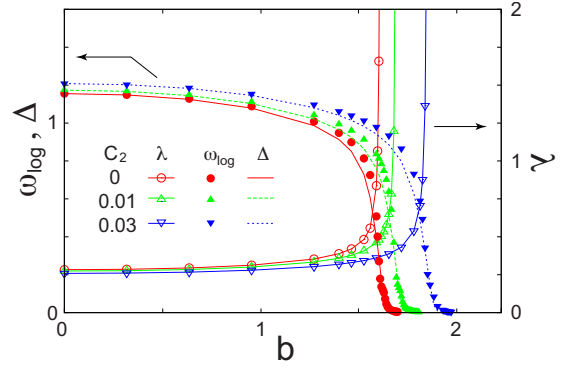
applied to our local phonon problem, we need care about the quantity $\lambda \langle \omega^2 \rangle$. As pointed out by Hardy and Flocken,[29] this quantity is related to the f-sum rule and this implies T_c is universal in any potential and depends only on the mass of the ion and α^2 as shown in Fig. 8. However, this is not true in our anharmonic phonon system. From numerical calculations, instead of $\langle \omega^2 \rangle$, we find that T_c for $b \gg b^*$ is approximately given by

$$T_c = 0.18 \Delta \sqrt{\lambda}. \tag{32}$$

We note that the origin of large λ for $b > b^*$ is the strong suppression of Δ for $b > b^*$ and other high-energy states do not play an important role. Thus, $\sqrt{\langle \omega^2 \rangle}$ overestimate the energy scale of T_c. These facts support the use of Δ instead of the averaged frequency $\sqrt{\langle \omega^2 \rangle}$.

F. Additional channel of attractive interactions

As we noted before, there is a crossover at $b = b^*$ to the quantum tunneling states and this means there are five states at low-energy region of the spectra as shown in Fig. 1. In the harmonic case, λ is basically determined by the matrix element $\langle n | x | 0 \rangle$ between the ground state $|0\rangle$ and the threefold-degenerate first excited states, and the corresponding excitation energy Δ. Since four low-energy excited states are nearly degenerate with the ground state around $b = b^*$, the singlet excited state $|s'\rangle$ also has a noticeable matrix element $\langle n | x | s' \rangle$. This provides another channel of attractive interaction and contributes to T_c. It is important to note that this additional contribution never appears in the one-dimensional model and is a direct consequence of the crossover of the ground state at $b = b^*$.

In Fig. 11, we show λ and the energy difference between s' state and the p-wavelike first excited states: $\Delta' = E_{s'} - E_p$. They are calculated with varying b, and plotted as a function of the energy difference Δ between the first excited state and the ground state. λ increases roughly as $\sim \Delta^{-3/4}$ for small Δ. Δ' shows minimum around $\Delta \sim 0.2$ and this reflects the anticrossing in the energy spectra. Corresponding to this, the coupling constant $\lambda_{s'}$ related to s' state shows a maximum around $\Delta \sim 0.1$ as shown in Fig. 12. Here, we define $\lambda_{s'}$ as
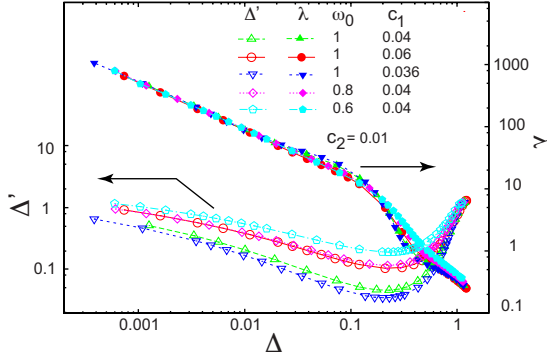
FIG. 11. (Color online) λ, Δ' vs Δ for $c_2=0.01$ and five sets of ω_0 and c_1. The open (filled) symbols represent Δ' (λ). Δ is controlled by varying b.

$$\lambda_{s'} = 2\alpha^2 \sum_{n=p} (w_n - w_{s'}) |\langle n|x|s'\rangle|^2 / (E_{s'} - E_n), \qquad (33)$$

where the n summation is taken over the three first excited states. Note that the smaller Δ' is, the larger $\lambda_{s'}$ is obtained. Depending on the magnitude of $\lambda_{s'}$, total λ has a small bump around the $\Delta \sim 0.1$ as a function of Δ. This observation clearly shows that there is a new channel of interaction via the excitations between the first excited states and the s' state.

G. Deviations from Allen-Dynes formula near $b=b^*$

As we discussed in Sec. III F, the enhancement of $\lambda_{s'}$ influences the total λ and also affects T_c itself. In Sec. III G, we derive a formula which includes the contribution of $\lambda_{s'}$. In order to take into account this contribution in Eq. (32), we assume the DOS given by

$$F(\omega) = \frac{\omega}{2} [\lambda_p \delta(\omega - \Delta) + \lambda_{s'} \delta(\omega - \Delta')]. \qquad (34)$$

Since the enhancement of $\lambda_{s'}$ takes place in a finite but extremely strong coupling regime, the total λ is large and we follow the discussion by Allen and Dynes to estimate the lower bound of T_c, by assuming a trial gap function
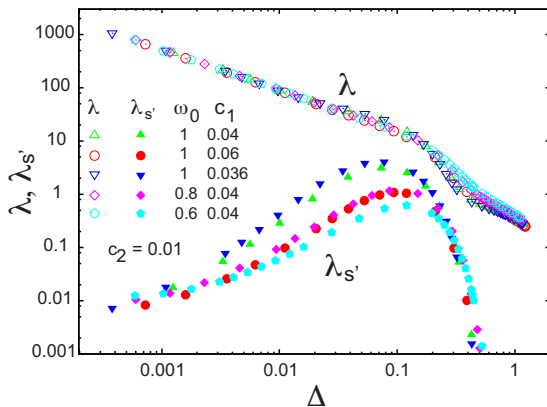

FIG. 12. (Color online) λ and $\lambda_{s'}$ vs Δ for $c_2=0.01$ and five sets of ω_0 and c_1. The open (filled) symbols represent λ ($\lambda_{s'}$).
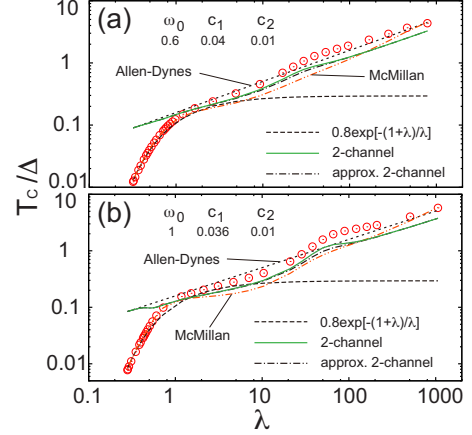
FIG. 13. (Color online) Various T_c formulas (27), (31), (35), and (36) vs λ. Formula (27) with $\omega_{\log}$ replaced by Δ is also plotted for comparison. (a) $\omega_0=0.6$, $c_1=0.04$, and $c_2=0.01$. (b) $\omega_0=1$, $c_1=0.036$, and $c_2=0.01$.

$\Delta_{SC}(i\omega_n) = \Delta_{SC}^0 \delta_{|\omega_n|, \pi T}$.[44] Using the form (34), we obtain the lower bound of T_c as

$$8\pi^2 T_c^2 = \lambda_p \Delta^2 + (\lambda_{s'} - 1)\Delta'^2$$
$$+ \sqrt{[\lambda_p \Delta^2 + (\lambda_{s'} - 1)\Delta'^2]^2 + 4(\lambda_p + \lambda_{s'})\Delta^2 \Delta'^2}. \qquad (35)$$

In the limit of $\lambda_{s'} \to 0$ Eq. (35) reduces to Eq. (32): $T_c = \Delta \sqrt{\lambda_p}/(2\pi)$. Although the more sophisticated gap function can give the almost correct coefficient 0.18 instead of $(2\pi)^{-1}$,[44] it is enough to consider the simplest trial gap function in order to examine the contributions of the s' state to T_c. In Eq. (35), we assume $\lambda_p(\geq 1)$ corresponds to the coupling constant originating from the transition between the ground state and p-wavelike states (first excited states) and $\lambda_{s'} \ll \lambda_p$ is the part from s' state [Eq. (33)]. Since $\lambda_p \gg \lambda_{s'}$, we can obtain a simpler approximate form of Eq. (35). This is obtained by simply replacing λ in Eq. (32) by λ_{eff},

$$\lambda_{\text{eff}} = \lambda_p \left[1 + \frac{\lambda_{s'}}{1 + 2\lambda_p \left(\frac{\Delta}{\Delta'}\right)^2} \right]. \qquad (36)$$

Figure 13 shows the λ dependence of T_c/Δ for two typical sets of parameters in log-log scale. As shown with the dashed line, the Allen-Dynes formula shows a straight line. For small λ, the calculated values agree with the McMillan's formula, while for extremely large λ they approach the line of the Allen-Dynes formula. For the intermediate $\lambda > 1$, however, the results show a bending and this bending is larger in Fig. 13(b) than in Fig. 13(a). Our two-channel formula (35) can describe the bending as indicated by the solid line. Although the lower bound of T_c, Eq. (35), is not in very good agreement with the calculated T_c, it captures the overall behavior of T_c for $\lambda > 1$. It is also noted that, although the McMillan's formula (27) shows an increase in T_c/Δ for large λ, the increase is too steep. The present two-component analysis confirms the existence of the additional channel of the interaction near the crossover point in this system.

IV. DISCUSSIONS

Let us now discuss the implications of our calculations to compare with characteristic properties experimentally observed in β-pyrochlore compounds. One point is the chemical trends among the three member compounds and we discuss why the potassium compound has the highest T_c of superconductivity. Another point is about the question why the superconducting phase is not so much affected by the isomorphic structure transition at T_p in the phase diagram. We will also propose a possible change in the K-oscillation profile at T_p and the effects of the transition on superconductivity.

A. Chemical trends in β-pyrochlore compounds

Among the three β-pyrochlore compounds AOs_2O_6 (A =K, Rb, or Cs), the K compound has the highest T_c^K =9.6 K of superconductivity and the strongest anharmonicity in the A-cation oscillation dynamics as observed in the neutron-scattering experiments: the Debye-Waller factor of K ion is much smaller than of Rb and Cs compounds[25] and the softening of the low-energy phonon peak is also the strongest in KOs_2O_6.[27] The Rb compound has the next strongest anharmonicity and the second highest T_c^{Rb}=6.3 K, while the Cs compound has the weakest anharmonicity and the lowest T_c^{Cs}=3.3 K. The ratio of T_c is approximately 3:2:1. Thus, the anharmonicity in the ion dynamics and the value of T_c are related. Let us examine this point in our results and also check if one can explain, at least qualitatively, the trends of other important quantities, electron mass enhancement and phonon energy.

A crucial difference among the three compounds is the size of A cation; the K ion has the smallest size, followed by Rb, and Cs is the biggest ion. Since the size of the surrounding $Os_{12}O_{18}$ cage essentially does not change, the K ion has the largest space inside the cage,[46] leading to strongly anharmonic oscillations. This reflects in different shapes of the A-cation potential, as shown in the calculation by Kuneš, *et al.*,[33] although the point-group symmetry is common.

In our theory, the compound-dependent potential shapes are modeled by adjusting parameters in the potential, Eq. (2) and (4). In the following, we will show that T_c values and the ion dynamics in the three compounds are naturally explained by appropriate choice of potential parameters. Throughout Sec. IV A, we will use some parameters explicitly shown with physical dimensions if necessary.

Let us first consider the trend of the value b/b^* among the three compounds, recalling the anharmonicity appearing in the Debye-Waller factor and the phonon energy observed in the neutron experiments.[25,27] As shown in Fig. 4, the anharmonicity grows with b/b^*. This implies that the b/b^* value is the smallest for Cs, then for Rb, and the largest for K. Note that the largest ratio is still smaller than or at most equal to the crossover value $b/b^*=1$, since the observed K-cation density profile does not change its peak position from the equilibrium position.[46,47]

Secondly, we consider the trend of the second-order potential parameter ω_0. Figure 14 shows the b dependence of T_c for several values of ω_0. The first-principle calculation of the
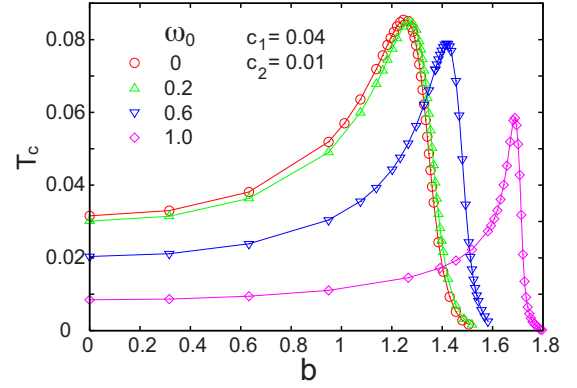

FIG. 14. (Color online) T_c vs b for five values of ω_0 fixing c_1 =0.04 and c_2=0.01.

ion potential clearly shows that ω_0 is very small for K while larger for Rb and the largest for Cs.[48] This trend is consistent with the fact that the K compound has the strongest anharmonicity and the highest T_c as far as $b<b^*$, as shown in Fig. 14. It is also important to note that the peak position $\sim b^*$ becomes smaller as ω_0 decreases.

By keeping these variations in b/b^* and ω_0 in mind, let us discuss our results of Δ, λ at $T=T_c$ and T_c itself for each of the three compounds. In order to make discussion simple, we assume the electron-phonon coupling and the electron density of states are the same for the three compounds and α^2 =1897 K/Å^2. The atomic mass of each A cation is M_K =71 748m_e, M_{Rb}=156 839m_e, and M_{Cs}=243 890m_e, respectively. We have adjusted potential parameters, Eq. (2), for each compound to reproduce the phonon energy and the effective ion oscillation variance $\langle x^2 \rangle_{exp}$ determined from the Debye-Waller factor.[25–27] As shown in Sec. II D, $W_d(\mathbf{Q})$ generally contains the contribution of the third-order fluctuations $\langle xyz \rangle$ in addition to $\langle x^2 \rangle$. However, since the experimental data is the $\mathbf{Q}$-averaged value of $\overline{W_d(\mathbf{Q})/|\mathbf{Q}|^2}$, it is sufficient to consider the second-order fluctuations $\langle W_d(\mathbf{Q})/|\mathbf{Q}|^2 \rangle$ $=\frac{1}{6}\langle |\mathbf{u}_d|^2 \rangle = \frac{1}{2}\langle x^2 \rangle$. Since our potential, Eq. (2) and (4), includes four parameters, we fix $B=9324$ K/Å^3 and $C_1=4C_2$ =3332 K/Å^4 for simplicity and vary Ω_0. It is noted that Ω_0 is expected to become smaller as the size of the alkali cation decreases, and, for fixed B, b/b^* becomes smaller as Ω_0 increases.

Table I shows the list of the basic quantities, Δ, λ, and T_c for the three compounds. Let us first discuss T_c. It is quite sure that one needs also to include a high-energy phonon, which plays a role to increase the T_c by about 3–5 K for all the three compounds, to obtain T_c consistent with the experimental results. $T_c^{(2)}$ is one calculated with including an additional phonon with energy $\hbar\Omega_h=260$ K. We have set the corresponding dimensionless coupling constant $\lambda_h=0.256$ in the calculations. The results of $T_c^{(2)}$ are quantitatively consistent with the experimental values $T_c^K=9.6$ K, $T_c^{Rb}=6.3$ K, and $T_c^{Cs}=3.3$ K. Here, we can reproduce the experimental values of T_c by assuming the same α^2, λ_h and Ω_h for all the three compounds and we conclude that the origin of the difference in T_c for the three β-pyrochlore compounds is due to the difference mainly in the anharmonicity of the alkali cation oscillations.[49]

TABLE I. Local potential parameters and $\langle x^2 \rangle$ at $T=0$, λ at $T=T_c$, Δ, T_c, and $T_c^{(2)}$ for the three β-pyrochlore compounds. The other parameters are $B=9324$ K/Å^3, $C_2=C_1/4=3332$ K/Å^4, and $\alpha^2=1897$ K/Å^2.

	$\hbar\Omega_0$ (K)	b/b^*	$\langle x^2 \rangle(T=0)$ (Å^2)	λ	Δ (K)	T_c (K)	$T_c^{(2)}$ (K)
K	26.4	0.58	0.0152	1.47	38.5	6.45	10.5
Rb	54.6	0.28	0.0050	0.34	56.2	0.82	5.74
Cs	74.8	0.11	0.0024	0.12	75.2	<0.03	3.37

Now, let us discuss the electron effective mass. In our theory, the electron mass enhancement factor is related to λ_{tot} as $1/z_{tot}=1+\lambda_{tot}$. λ's obtained from experiments and previous theoretical studies are $\lambda^K=1.6-2.4$,[3,17,20,22] for K, $\lambda^{Rb}=1.0-1.3$,[20,32] for Rb and $\lambda^{Cs}=0.78$,[20] for Cs, respectively. Our estimation of $\lambda_{tot}=\lambda+\lambda_h=\lambda+0.256$ with λ in Table I is qualitatively consistent with these values, although we have not fit T_c for each compound. The experimental values of specific-heat coefficient γ is $\gamma_K=70$, $\gamma_{Rb}=45$, and $\gamma_{Cs}=41$ mJ/mol K^2 while the band calculations predicted $\gamma_0 \sim 10$ mJ/mol K^2 for all the three compounds.[20,50] Thus, the experimental mass enhancement factor γ_K/γ_0 in KOs$_2$O$_6$ is 1.5–1.7 times larger than in RbOs$_2$O$_6$ and CsOs$_2$O$_6$.[51] In our calculation, $z_{tot}^{Rb}/z_{tot}^K \simeq 1.71$ and $z_{tot}^{Cs}/z_{tot}^K \simeq 1.98$, which are semiquantitatively consistent with the experimental values. From our results, the enhanced mass enhancement in KOs$_2$O$_6$ is attributed to the proximity to the crossover to the quantum tunneling state and also the large oscillation amplitude, which effectively enhances the electron-phonon coupling.

In order to obtain the correct value of the mass enhancement (~ 7 for KOs$_2$O$_6$ and ~ 4 for the other two), we should also take into account the electron-electron interactions, but this is beyond the scope of the present study and we leave it for a future problem. Nevertheless, it is important to note that λ is significantly enhanced near $b=b^*$ by anharmonic oscillations and that this is the central reason why the mass enhancement in KOs$_2$O$_6$ is much larger than in Rb and Cs compounds.

As for the phonon frequency Δ, optical modes related to the A-cation oscillations are observed at energy around 5–7 meV at room temperature in the inelastic neutron scattering[25,27] and their energies show strong softening as the temperature decreases. This corresponds to our results shown in Fig. 7. For KOs$_2$O$_6$, the phonon energy at $T=1.5$ K is about 3.1 meV, which is quite small compared with the value of 5.5 meV at $T=300$ K.[27] Furthermore, the low-energy phonon peaks in KOs$_2$O$_6$ are rather broad compared with Rb and Cs compounds,[27] which suggests the proximity to the crossover point. The specific-heat experiment[3] and the photoemission spectroscopy data[52] also support these results.

In our calculation for KOs$_2$O$_6$ with parameters in Table I, the peak position in the phonon spectrum is about 70 K $\simeq 6$ meV at $T=300$ K and this shifts to $\Delta=38.5$ K as T decreases. This means the potential parameters in Table I can reproduce not only T_c and Δ but also the temperature dependence of the spectra.

As for the chemical trends, we have calculated superconducting transition temperature for the three β-pyrochlore

compounds adjusting parameters in the potential, Eq. (2), and we can reproduce the phonon energy and amplitude related to the average Debye-Waller factor. We have obtained quantitatively consistent values of T_c with the experimental ones, using the same electron-phonon coupling, the electron DOS and also the same additional high-energy phonon for all the three compounds.

B. Changes at T_p

As mentioned in Sec. I, KOs$_2$O$_6$ exhibits an isomorphic first-order transition at $T_p=7.5$ K.[3,4,47] In Sec. IV B, let us investigate the effects of this transition on the phonon dynamics, using a set of constraints offered by the experimental results. We also discuss its effects on superconductivity.

Electric resistivity shows a concave temperature dependence at high temperatures and this is attributed to the strong coupling to phonons with strong anharmonicity.[3,23] At the magnetic field $H=14$ T, the resistivity is suddenly suppressed by 25% at T_p, and shows a different T dependence proportional to T^2 at $T_c<T<T_p$.[3] This indicates that the electron-phonon scattering processes are reduced significantly at T_p.[3] This is also consistent with the reduction in the specific-heat jump at T_c in magnetic fields above 8 T.[3]

In the magnetic field-temperature phase diagram, T_p remains essentially insensitive to magnetic field H as shown in Fig. 15. The upper critical magnetic field H_{c2} is suppressed below T_p, but extrapolating to the region above T_p, it seems that it also vanishes at the position very close to $T_c(H=0)$.

This fact cannot be explained if the characteristic energy scale, ω_{log} or Δ is common across T_p: the extrapolated H_{c2} line should vanish below $T_c(H=0)$ since λ is reduced below
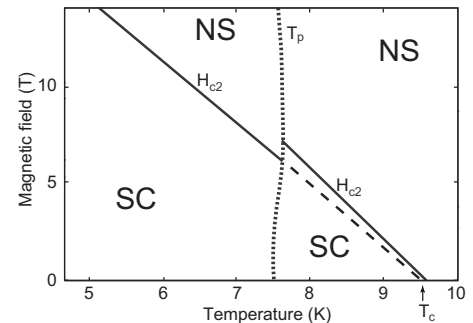

FIG. 15. Schematic temperature-magnetic field phase diagram taken from Ref. 3. The solid and dotted lines represent H_{c2} and T_p, respectively. The dashed line indicates the extrapolation of low-T H_{c2} to the higher-temperature region.
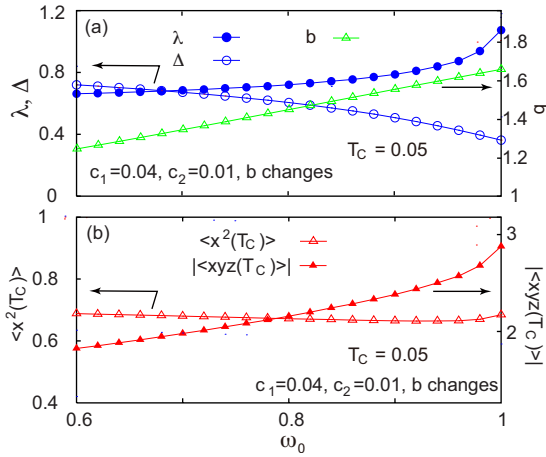
FIG. 16. (Color online) ω_0 dependence of characteristic quantities, when T_c is fixed to 0.05 by tuning b. (a) λ, Δ, and b. (b) The second- and third-order moments of ion oscillation $\langle x^2 \rangle$ and $|\langle xyz \rangle|$. $c_1 = 0.04$ and $c_2 = 0.01$.

T_p as discussed above. Therefore, the above fact implies the enhancement of the characteristic energy scale Δ or $\omega_{\log}$ below T_p. Indeed, Chang, *et al.*,[22] assumed a slightly increased Einstein energy to fit the specific-heat data and our previous study also predicted the increase in the oscillation energy.[34]

Let us discuss the changes in λ, Δ, $|\langle x^2 \rangle|$, and $|\langle xyz \rangle|$ at T_p based on our results, modeling the isomorphic transition by a sudden change in the two potential parameters, ω_0 and b. This change corresponds to the variation in the mean-field part of intersite ion interactions, which was discussed in Ref. 34 and also changes in the oxygen positions and the lattice constant.[47] Two parameters are chosen under the constraints (i) two different parameter sets above and below T_p lead to the same T_c, and (ii) λ is smaller below T_p, both of which are the experimental constraints, and we also assume (iii) no significant change in the electron band structure across the transition and thus α^2 is also unchanged, and (iv) $b < b^*$ for both below and above T_p implied by the result of the electron-density profile obtained by the x-ray and the neutron experiments[46,47] as discussed before. In the following, we discuss the change across T_p based on these constraints.

In Fig. 16, characteristic quantities are shown for fixed c_1 and c_2 with varying ω_0 and simultaneously b such that those give the same $T_c = 0.05$. Since $b < b^*$ which is the assumption (iv), T_c is well approximated by the McMillan formula (27), in which T_c is determined by the two factors $\omega_{\log} \simeq \Delta$ and λ.

Firstly, it is noted that λ increases as ω_0 increases. One might expect a suppression of λ as ω_0 increases but the key point is that we simultaneously tune b to fix T_c unchanged and this means larger b is necessary at larger ω_0. This increase in b overcomes the competing effect of the increase in ω_0, and finally λ increases. Secondly, the energy of the first excited state Δ increases as ω_0 decreases. This is naturally understood by noting that Δ becomes large for smaller b. Thus, from the constraint (ii) the above results imply that the phonon energy is enhanced below T_p and, indeed, this is consistent with the previous theoretical studies.[22,34]

Most interestingly, the second- and third-order fluctuations $\langle x^2 \rangle$ and $|\langle xyz \rangle|$ change oppositely as shown in Fig.
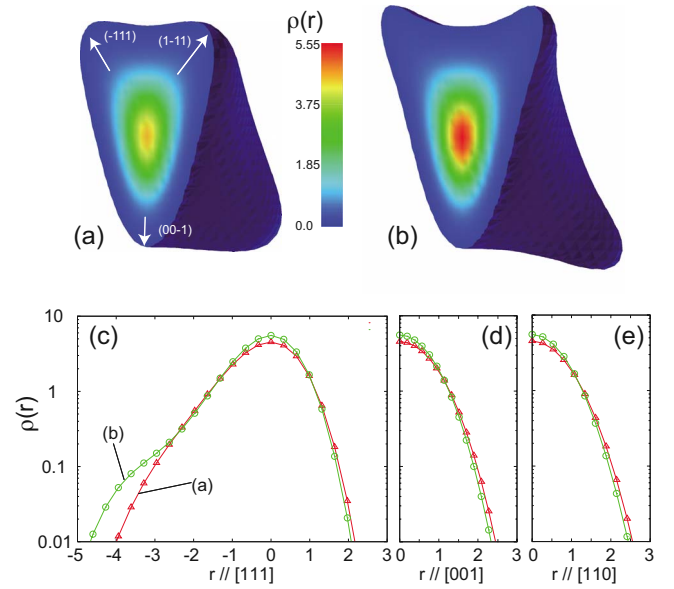

FIG. 17. (Color online) Ion density isosurface for $\rho(\mathbf{r}) = 0.05$ and the density map on the section with (110) plane at $T = 0.002$. (a) $\omega_0 = 0.8$, $b = 1.44$ and (b) $\omega_0 = 1$, $b = 1.66$. (c) $\rho(\mathbf{r})$ along [111] direction corresponding to (a) and (b), (d) along [001] and (e) along [110] direction. $\rho(-|\mathbf{r}|)$'s in (d) and (e) are not shown since $\rho(\mathbf{r}) = \rho(-\mathbf{r})$ along these directions.

16(b). As ω_0 decreases, $\langle x^2 \rangle$ increases for the most of the ω_0 range, while $|\langle xyz \rangle|$ decreases monotonically. This is because small ω_0 corresponds to small b as explained above. These results indicate that $\langle x^2 \rangle$ is slightly enhanced below T_p while $|\langle xyz \rangle|$ is suppressed.

In order to illustrate these anisotropic fluctuations, the density isosurface for $\rho(\mathbf{r}) = 0.05$ and the density (color) map are shown for two different parameters at $T = 0.002$ in Fig. 17: for (a) and (b), $\omega_0 = 0.8$ and 1.0, and $b = 1.44$ and 1.66, respectively, and these two sets give the same $T_c = 0.045$, and we choose the two parameter sets to emphasize the change in the oscillation profile. As expected from the values of b, the case (a) has the smaller $\lambda = 0.647$ and the larger $\Delta = 0.662$, while $\lambda = 0.782$ and $\Delta = 0.429$ for the case (b).

One can see that the density isosurface shows more anisotropic character in the case (b), where the "spikes" sticking out along four [111] directions are sharper than those in the case (a). This aspect reflects in the values of $\langle x^2 \rangle$ and $\langle xyz \rangle$. Indeed, $\langle x^2 \rangle$ at $T = T_c$ is larger $\langle x^2 \rangle = 0.645$ in (a) than 0.626 in (b), while $|\langle xyz \rangle|$ at $T = T_c$ is smaller $|\langle xyz \rangle| = 1.93$ in (a) than 2.35 in (b). Figures 17(c)–17(e) show $\rho(\mathbf{r})$ along [111], [001], and [110] directions, respectively, for the same two data. It is clearly seen that $|\langle xyz \rangle|$ in (b) is larger than that in (a) as shown in (c), and $\langle x^2 \rangle$ in (a) is larger than in (b) as shown in (d) and (e).

These changes in the anisotropy of density distribution is a characteristic nature of the first-order isomorphic transition at T_p. This transition is isomorphic, consistent with the experiments,[3,4] because the amplitude of anisotropy changes but it does not break the point group, translational, and any other symmetries. Our results suggest that $\langle x^2 \rangle$ is slightly enhanced while $|\langle xyz \rangle|$ is suppressed below T_p in KOs_2O_6. Recent high-resolution neutron-scattering experiment shows

the increase in $\langle x^2 \rangle$ across T_p as T decreases,[47] which is consistent with our result.

Furthermore, although it is naively expected that an increase in $\langle x^2 \rangle$ corresponds to the enhancement of λ, this does not necessarily hold in this system, since the value of λ is sensitive to the value of b, especially near the crossover point b^*. Our results show that the value of $|\langle xyz \rangle|$ plays more important role for the enhancement of λ than $\langle x^2 \rangle$. In order to detect this change in the density distribution across T_p, it is important to perform detailed neutron-scattering experiments and to analyze the results with taking into account the third-order term in Debye-Waller factor as discussed in Sec. II D. It is worthwhile to examine the **Q** dependence of the Debye-Waller factor to extract the anisotropy of the oscillations since **Q**-averaged Debye-Waller factor hinders the anisotropy and anharmonicity.

Finally, we comment on the possibility of re-entrant superconducting transition. Experimentally, Hiroi *et al.*,[3] observed a re-entrant superconducting transition around H $=7$ T as shown in Fig. 15. This can be understood from $H_{c2}(T=0)$ in the strong coupling theory of superconductivity,

$$H_{c2}(T=0) \propto T_c^2 (1+\lambda)^2 \left(1 + 1.44 \frac{T_c}{\omega_{\log}} + \cdots\right), \quad (37)$$

for the clean limit.[53] In our analysis, the λ decreases and $\omega_{\log}$ increases below T_p, while the T_c is approximately the same for the potential parameters above and below T_p. Thus, $H_{c2}(T=0)$ for the low-T parameter set is smaller than that for the high-T set. Therefore, we expect a $H_{c2}(T)$ curve similar to that shown in Fig. 15. This result does not change when we use the formula for the dirty limit.[53]

V. SUMMARY

We have investigated in the present paper anharmonic phonons and strong coupling superconductivity in β-pyrochlore compounds, AOs$_2$O$_6$ (A=K, Rb, or Cs). First, we have solved the Schrödinger equation of the three-dimensional anharmonic phonon in tetrahedral symmetry. The main issue is the importance of the third-order anharmonicity $bxyz$ in the ion potential allowed for this symmetry. We have determined the energy spectrum of the anharmonic phonon as a function of the third-order anharmonicity b. We have found that there exists a crossover of the ground state to the quantum tunneling state for $b > b^*$. We have pointed out nonmonotonic temperature dependence of ion density profile near the crossover point b^*.

Secondly, we have calculated the transition temperature of superconductivity T_c mediated by these anharmonic phonons. We have found that the enhancement of T_c near b $=b^*$. Its b dependence can be well fitted by the McMillan formula at $b \lesssim b^*$. For $b \gtrsim b^*$ we have found that there exists an additional channel of pairing interaction, which turns out to originate from low-energy excited states appearing at b $\sim b^*$. We have analyzed its contribution and derived an approximated formula of T_c in the strong coupling limit.

We have also discussed the chemical trends of T_c in the β-pyrochlore family AOs$_2$O$_6$ (A=K, Rb, or Cs). The main difference among the three members are different values of b/b^* and the second-order term in the ion potential ω_0. By assuming the same electron-phonon coupling constant α^2 and the same high-energy phonon for all the three compounds, the differences in T_c and the energy of the first excited phonon states Δ have been quantitatively explained only by the difference in the local anharmonic potential.

Finally, we have discussed the effect of the first-order transition observed in KOs$_2$O$_6$. The changes in the density distribution of K cation at the first-order transition have been discussed based on the experimental data obtained so far. Especially, we have found that $\langle x^2 \rangle$ and $|\langle xyz \rangle|$ change differently across T_p. Our results suggest the increase in the first excited phonon energy Δ and the reduction in the dimensionless electron-phonon coupling constant λ across T_p. While the latter is consistent with the experimental results, the former has not been observed and this is our prediction for the experiments. In order to detect the increase in Δ, it is important to carry out the high-resolution inelastic neutron-scattering experiments. We hope our results shed lights in β-pyrochlore compounds both on the strong coupling superconductivity and on the anharmonic oscillations observed.

*hattori@issp.u-tokyo.ac.jp

[1] Z. Hiroi, S. Yonezawa, and Y. Muraoka, J. Phys. Soc. Jpn. **73**, 1651 (2004).

[2] Z. Hiroi, S. Yonezawa, J. Yamaura, T. Muramatsu, and Y. Muraoka, J. Phys. Soc. Jpn. **74**, 1682 (2005).

[3] Z. Hiroi, S. Yonezawa, Y. Nagao, and J. Yamaura, Phys. Rev. B **76**, 014523 (2007).

[4] T. Hasegawa, Y. Takasu, N. Ogita, M. Udagawa, J. I. Yamaura, Y. Nagao, and Z. Hiroi, Phys. Rev. B **77**, 064303 (2008).

[5] T. Goto, Y. Nemoto, K. Sakai, T. Yamaguchi, M. Akatsu, T. Yanagisawa, H. Hazama, K. Onuki, H. Sugawara, and H. Sato, Phys. Rev. B **69**, 180511(R) (2004).

[6] K. Kaneko, N. Metoki, H. Kimura, Y. Noda, T. D. Matsuda, and M. Kohgi, J. Phys. Soc. Jpn. **78**, 074710 (2009).

[7] H. Kotegawa, H. Hidaka, T. C. Kobayashi, D. Kikuchi, H. Sugawara, and H. Sato, Phys. Rev. Lett. **99**, 156408 (2007).

[8] B. C. Sales, B. C. Chakoumakos, R. Jin, J. R. Thompson, and D. Mandrus, Phys. Rev. B **63**, 245113 (2001).

[9] I. Zerec, V. Keppens, M. A. McGuire, D. Mandrus, B. C. Sales, and P. Thalmeier, Phys. Rev. Lett. **92**, 185502 (2004).

[10] H. Matsumoto, T. Mori, K. Iwamoto, S. Goshima, S. Kushibiki, and N. Toyota, Phys. Rev. B **79**, 214306 (2009).

[11] Y. Kasahara, Y. Shimono, T. Shibauchi, Y. Matsuda, S. Yonezawa, Y. Muraoka, and Z. Hiroi, Phys. Rev. Lett. **96**, 247004 (2006).

[12] M. Yoshida, K. Arai, R. Kaido, M. Takigawa, S. Yonezawa, Y. Muraoka, and Z. Hiroi, Phys. Rev. Lett. **98**, 197002 (2007).

[13] Y. Nakai, K. Ishida, H. Sugawara, D. Kikuchi, and H. Sato, Phys. Rev. B **77**, 041101(R) (2008).

[14] Y. Nemoto, T. Yamaguchi, T. Horino, M. Akatsu, T. Yanagisawa, T. Goto, O. Suzuki, A. Dönni, and T. Komatsubara, Phys. Rev. B **68**, 184109 (2003).

[15] I. Ishii, T. Fujita, I. Mori, H. Sugawara, M. Yoshizawa, K. Takegahara, and T. Suzuki, J. Phys. Soc. Jpn. **78**, 084601 (2009).

[16] Y. Nakanishi and M. Yoshizawa (private communications).

[17] M. Brühwiler, S. M. Kazakov, J. Karpinski, and B. Batlogg, Phys. Rev. B **73**, 094518 (2006).

[18] I. Bonalde, R. Ribeiro, W. Brämer-Escamilla, J. Yamaura, Y. Nagao, and Z. Hiroi, Phys. Rev. Lett. **98**, 227003 (2007).

[19] Y. Shimono, T. Shibauchi, Y. Kasahara, T. Kato, K. Hashimoto, Y. Matsuda, J. Yamaura, Y. Nagao, and Z. Hiroi, Phys. Rev. Lett. **98**, 257004 (2007).

[20] Y. Nagao, J. Yamaura, H. Ogusu, Y. Okamoto, and Z. Hiroi, J. Phys. Soc. Jpn. **78**, 064702 (2009).

[21] J. Chang, I. Eremin, P. Thalmeier, and P. Fulde, Phys. Rev. B **76**, 220510(R) (2007).

[22] J. Chang, I. Elemin, and P. Thalmeier, New J. Phys. **11**, 055068 (2009).

[23] T. Dahm and K. Ueda, Phys. Rev. Lett. **99**, 187003 (2007).

[24] A. Yamakage and Y. Kuramoto, J. Phys. Soc. Jpn. **78**, 064602 (2009).

[25] K. Sasai, K. Hirota, Y. Nagao, S. Yonezawa, and Z. Hiroi, J. Phys. Soc. Jpn. **76**, 104603 (2007).

[26] R. Galati, C. Simon, P. F. Henry, and M. T. Weller, Phys. Rev. B **77**, 104523 (2008).

[27] H. Mutka, M. M. Koza, M. R. Johnson, Z. Hiroi, J. I. Yamaura, and Y. Nagao, Phys. Rev. B **78**, 104307 (2008).

[28] N. M. Plakida, V. L. Aksenov, and S. L. Drechsler, Europhys. Lett. **4**, 1309 (1987).

[29] J. R. Hardy and J. W. Flocken, Phys. Rev. Lett. **60**, 2191 (1988).

[30] V. H. Crespi and M. L. Cohen, Phys. Rev. B **48**, 398 (1993).

[31] G. D. Mahan and J. O. Sofo, Phys. Rev. B **47**, 8050 (1993).

[32] S. Manalo, H. Michor, G. Hilscher, M. Brühwiler, and B. Batlogg, Phys. Rev. B **73**, 224520 (2006).

[33] J. Kuneš, T. Jeong, and W. E. Pickett, Phys. Rev. B **70**, 174510 (2004); J. Kuneš and W. E. Pickett, Physica B **378-380**, 898 (2006).

[34] K. Hattori and H. Tsunetsugu, J. Phys. Soc. Jpn. **78**, 013603 (2009).

[35] In those cases of $\omega_0 \neq 1$, we keep the same energy unit of 44 K, instead of renormalization of energy. This simplifies our discussions about ω_0 dependence in later sections.

[36] S. W. Lovesey, *Theory of Neutron Scattering from Condensed Matter* (Clarendon Press, Oxford, 1984), Vol. 1.

[37] K. Hattori and K. Miyake, J. Phys. Soc. Jpn. **76**, 094603 (2007).

[38] M. Takechi and K. Ueda, J. Phys. Soc. Jpn. **78**, 024604 (2009).

[39] G. M. Eliashberg, Zh. Eksp. Teor. Fiz. **38**, 966 (1960) [Sov. Phys. JETP **11**, 696 (1960)].

[40] D. J. Scalapino, J. R. Schrieffer, and J. W. Wilkins, Phys. Rev. **148**, 263 (1966).

[41] A. A. Abrikosov, L. P. Gorkov, and I. Y. Dzyaloshinskii, *Quantum Field Theoretical Methods in Satistical Physics*, 2nd ed. (Pergamon Press, Oxford, 1965).

[42] G. Bergmann and D. Rainer, Z. Phys. **263**, 59 (1973).

[43] W. L. McMillan, Phys. Rev. **167**, 331 (1968).

[44] P. B. Allen and R. C. Dynes, Phys. Rev. B **12**, 905 (1975).

[45] When λ is expressed by the quantities with the dimension, $\lambda = (2\alpha^2/\Delta)(\hbar/2M\Delta)$, which is, indeed, dimensionless.

[46] J. Yamaura, S. Yonezawa, Y. Muraoka, and Z. Hiroi, J. Solid State Chem. **179**, 336 (2006).

[47] K. Sasai, M. Kofu, R. M. Ibberson, K. Hirota, J. Yamaura, Z. Hiroi, and O. Yamamuro, J. Phys.: Condens. Matter **22**, 015403 (2010).

[48] The result in Ref. 33 suggests a slightly negative value of ω_0 for KOs_2O_6. However, the first excited state then has an energy too small compared with the experimental estimate from the specific heat data (Ref. 3) and the neutron scattering (Refs. 25 and 27). Correspondingly, calculated $\langle x^2 \rangle$ is too large compared with the experimental results and its temperature dependence is qualitatively different from the experimental one (Refs. 25 and 26). In this paper, we consider the cases of $\omega_0 \geq 0$ for simplicity. We hope that more detailed information on the ion potential is provided by the neutron-scattering experiments in the future.

[49] In this point whether the additional phonon is acoustic or optical mode does not make an essential difference. To improve estimation of T_c, we need the detailed information of each compound on the electron-phonon coupling α^2, Ω_h, λ_h, and other parameters.

[50] Z. Hiroi, J. Yamaura, S. Yonezawa, and H. Harima, Physica C **460-462**, 20 (2007).

[51] Note that this value of the mass enhancement factor includes not only the contributions of electron-phonon interactions but also those of electron-electron interactions.

[52] T. Shimojima, Y. Shibata, K. Ishizaka, T. Kiss, T. Tagoshi, A. Chainani, T. Yokoya, X.-Y. Wang, C. T. Chen, S. Watanabe, J. Yamaura, S. Yonezawa, Y. Muraoka, Z. Hiroi, T. Saitoh, and S. Shin, Phys. Rev. Lett. **99**, 117003 (2007).

[53] J. P. Carbotte, Rev. Mod. Phys. **62**, 1027 (1990).